Validation of the Two-Region Rossi-alpha Model for Reflected Assemblies

Michael Y. Hua[a,b], Flynn B. Darby[a], Jesson D. Hutchinson[b], George E. McKenzie[b], Shaun D. Clarke[a], Sara A. Pozzi[a]

[a] *Department of Nuclear Engineering and Radiological Sciences, University of Michigan, Ann Arbor, MI 48109*
[b] *NEN-2: Advanced Nuclear Technology Group, Los Alamos National Laboratory, Los Alamos, NM 87545*

Abstract

Nuclear criticality safety, nonproliferation and safeguards, emergency response, and stockpile stewardship utilize estimates of the k_{eff} multiplication factor. The value of k_{eff} cannot be directly measured, but it can be inferred from the prompt neutron period. One modality of measuring the prompt neutron period is the Rossi-alpha method, which is predicated on fitting a histogram of detection time differences due to the nonrandom temporal distribution of same-fission-chain neutrons. Recent works have developed the motivation and theory to expand traditional one-region point kinetic models resulting in one-exponential histogram fits to two-region models that result in two-exponential fits. This paper validates the new two-region model using organic scintillator measurements of copper-reflected weapons-grade plutonium ($0.83 \leq k_{\text{eff}} \leq 0.94$) and high-density-polyethylene-reflected highly enriched uranium ($0.73 \leq k_{\text{eff}} \leq 0.95$). Furthermore, the results show that more thermal systems have shorter prompt neutron periods in the core region due to increased induced-fission probabilities for moderated neutrons. A new parameter introduced by the two-region model is also shown to be correlated to the amount of reflection, and may be used to infer assembly properties such as type and amount of reflector.

Keywords:
Rossi-alpha, Neutron Noise, Prompt Neutron Decay Constant, Prompt Period, Subcritical Measurements, Validation, Two-Exponential

1. Introduction

The Rossi-alpha method is a neutron noise technique for near- and delayed-critical assemblies of fissile material and one modality to estimate the prompt neutron decay constant or its negative reciprocal, the prompt neutron period [1–4]. The method exploits the nonrandom distribution of neutron detection times due to the correlations between same-fission-chain neutrons; neutron detection times are tabulated in experiment, a histogram of time differences between detections is constructed, and the histogram is fit with a function that defines the prompt neutron period [5, 6]. The prompt period is typically used to infer the k_{eff} multiplication factor of a given assembly, which has far-reaching applications in nuclear criticality safety, safeguards and nonproliferation, and stockpile stewardship. The Rossi-alpha method was originally developed for bare cores of fissile material where a one-region point kinetics model resulting in a one-exponential function is an adequate fit for the histogram and correctly captured the dominant time correlations [5, 7]. Recent work demonstrated that a two-region point kinetics model resulting in a two-exponential function is (and that a one-exponential function is not) an adequate fit of Rossi-alpha histograms from reflected assemblies of fissile material [8, 9] and other work developed the theory to calculate the prompt period from the fit parameters [10–12]. The purpose of this manuscript is to validate the two-region point kinetics model for Rossi-alpha experiments.

The outline of this manuscript is as follows. The Rossi-alpha and two-region point kinetics theory are reviewed in Sec 2. The experiments are described in Sec. 3, analysis of the data is outlined in Sec. 4, and the subsequent results are discussed in Sec. 5. A dedicated simulation study is presented in Sec. 6 and the paper is concluded in Sec. 7.

2. Background: The Two-Exponential Rossi-alpha Method

The prompt neutron decay constant α is defined as the negative asymptotic logarithmic time derivative of the prompt neutron population N_p in the fissile core and given by [4, 13]

$$\alpha = -\frac{d(\ln(N_p(t)))}{dt} = -\frac{1}{N_p(t)}\frac{d(N_p(t))}{dt}. \tag{1}$$

When one-region point kinetics is adequate, Rossi-alpha histograms are fit with

$$p(t)\ dt = A\ dt + Be^{\alpha t}\ dt, \tag{2}$$

where the A term represents the uniform probability of chance coincidences and the B term represents the exponential decay of the prompt neutron population as fission chains extinguish. The k_{eff} multiplication factor is inferred from α by

$$k_{\text{eff}} = \frac{1}{1 - \beta_{\text{eff}} + \alpha\Lambda}, \tag{3}$$

where β_{eff} is the effective delayed neutron fraction and Λ is the mean neutron generation time. The values of β_{eff} and Λ are estimated from simulation or approximated with repeated pertubation measurements; in the simulation code MCNP®[1], solving for the point kinetics quantities can be invoked with the KOPTS option of the KCODE subroutine.

When the two-region model is needed due to reflection, the measured α corresponds to the core only and not the composite assembly. Therefore $k_{\text{eff,core}}$ is calculated based on a simulated value of Λ_{core} (the KOPTS option results in a value for the composite assembly instead) or a simulated value of the mean neutron lifetime in the core, τ_c. In either case, β_{eff} is still needed. In the τ_c approach, the prompt multiplication factor of the core $k_{p,\text{core}}$ is calculated from α and τ_c by

$$\alpha = \frac{k_{p,\text{core}} - 1}{\tau_c} \iff k_{p,\text{core}} = 1 + \alpha\tau_c \tag{4}$$

and the effective multiplication factor of the core is calculated from $k_{p,\text{core}}$ and β_{eff} by

$$k_{\text{eff,core}} = \frac{k_{p,\text{core}}}{1 - \beta_{\text{eff}}}. \tag{5}$$

The composite k_{eff} is calculated by considering cross-region leakage terms: f_{cr}, the fraction of neutrons leaking from the core to the reflector, and f_{rc}, the fraction of neutrons leaking from the reflector to the core. Taken together,

[1]MCNP® and Monte Carlo N-Particle® are registered trademarks owned by Triad National Security, LLC, manager and operator of Los Alamos National Laboratory. Any third party use of such registered marks should be properly attributed to Triad National Security, LLC, including the use of the designation as appropriate. For the purposes of visual clarity, the registered trademark symbol is assumed for all references to MCNP within the remainder of this paper.

$$
\begin{aligned}
k_{\text{eff}} &= \frac{k_{\text{eff,core}}}{1 - f_{rc} f_{cr}} \\
&= \frac{k_{\text{eff,core}}}{1 - f' \tau_c} \\
&= \frac{k_{p,\text{core}}}{(1 - f' \tau_c)(1 - \beta_{\text{eff}})} \\
&= \frac{1 + \alpha \tau_c}{(1 - f' \tau_c)(1 - \beta_{\text{eff}})},
\end{aligned} \tag{6}
$$

where

$$
f' = \frac{f_{cr} f_{rc}}{\tau_c} \tag{7}
$$

is defined since f' is a measured value and the individual cross-region leakage terms cannot be independently determined in experiment. Hence, k_{eff} is determined from two measured values, α and f', and two simulated values, β_{eff} and τ_c.

The two-exponential fit is given by

$$
\begin{aligned}
p(t)\ dt &= A\ dt + B \left[\rho_1 e^{r_1 t} + \rho_2 e^{r_2 t} \right]\ dt \\
&= A\ dt + \left[(B\rho_1) e^{r_1 t} + (B\rho_2) e^{r_2 t} \right]\ dt
\end{aligned} \tag{8}
$$

where A and B respectively correspond to the uncorrelated and correlated terms, and the coefficients are given by

$$
\rho_1 = \frac{(1-R)^2}{r_1} + \frac{2(1-R)(R)}{r_1 + r_2} \tag{9a}
$$

and

$$
\rho_2 = \frac{R^2}{r_2} + \frac{2(1-R)(R)}{r_1 + r_2}, \tag{9b}
$$

and the exponents are related to macroscopic quantities by

$$
r_j = (-1)^j \sqrt{\frac{1}{\tau_r} \left(f' + \alpha \right) + \frac{1}{4} \left(\frac{1}{\tau_r} - \alpha \right)^2} + \frac{1}{2} \left(\alpha - \frac{1}{\tau_r} \right). \tag{10}
$$

The parameter τ_r is the mean time in the reflector (mean time outside of the core) and R is a number between zero and one that weights the exponents to determine α:

$$\alpha = r_1(1-R) + r_2(R). \quad (11)$$

The value of f' is similarly calculated and given by:

$$f' = -\frac{(\alpha - r_1)(\alpha - r_2)}{\alpha - r_1 - r_2}. \quad (12)$$

Note that the true value of τ_r is rarely measured and dependent on the detection system being used.

3. Experimental Setup

The two-region model is validated with experimental data from uranium and plutonium by comparing measured values to simulated values, which are treated as the reference in this work. The experiments were performed at the National Criticality Experiments Research Center within the Device Assembly Facility at the Nevada National Security Site. The front face of each detection system was 47 cm from the center of the radiation test object; the layout and detection systems are identical to those of Ref. [14] and a photo is shown in Fig. 1. Two types of detection systems were present during the experiments: two organic scintillator arrays [14] (12 5.08-cm thick, 5.08-cm diameter *trans*-stilbene crystals [16, 17]) and two Neutron Multiplicity ^{3}He Array Detectors (NoMADs, extensively reviewed in Ref. [15]). Rossi-alpha measurements are typically conducted with ^{3}He detectors: ^{3}He-gas proportional counters embedded in a polyethylene matrix to moderate neutrons and improve detection efficiency. Such systems have clock tick lengths on the order of hundreds of nanoseconds, dead times on the order of several microseconds, and characteristic slowing-down times on the order of tens of microseconds [15]. When measuring the same copper-reflected plutonium assemblies as this work, the only time constant ^{3}He detectors were sensitive to were their own slowing down time of 35-40 μs [15]. Therefore only data from the organic scintillator array (time resolution of 1.34 ns, negligible dead time, and clock tick lengths of approximately 0.3 ns) are used in this work.

The organic scintillators are coupled to photomultiplier tubes and held in place by porous foam in a thin wire-frame housing. The detectors were powered and read out by CAEN V6533N high voltage supplies and v1730 digitizers that sampled every 2 ns for a record length of 144 samples.

Graded tin-copper shadow shields were placed in front of the organic scintillator arrays to shield low-energy x-rays.

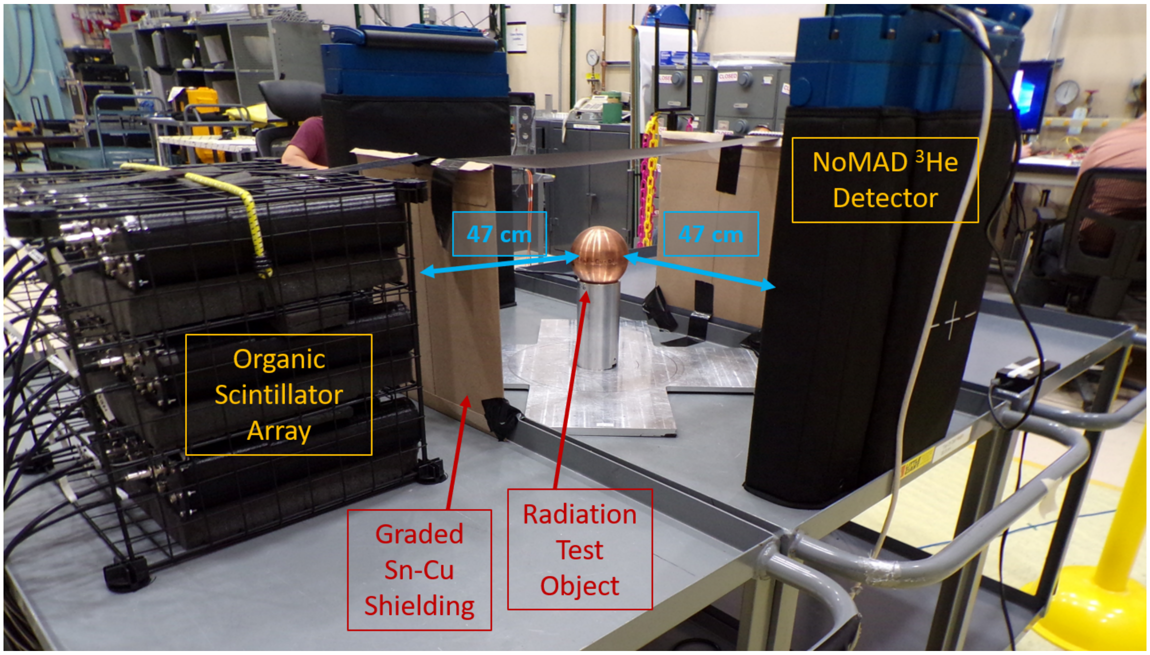

Figure 1: Annotated layout of detection systems and measurement setup.

The plutonium assembly uses a 4.5-kg sphere of weapons-grade (93% ^{239}Pu), alpha-phase plutonium encased in stainless steel known as the BeRP Ball [18, 19]. The BeRP Ball has recently been used in several benchmark measurements that comprehensively specify the object and provide detailed MCNP input files [15, 20, 21]. The measurements in this work replicate the copper-only configurations of the subcritical copper-reflected α-phase plutonium (SCRαP) benchmark [15], where the BeRP Ball is reflected by tight-fitting copper shells with thicknesses ranging from 1.27 cm to 10.16 cm in 1.27 cm increments. Photos of the configurations are shown in Fig. 2. Each configuration was measured for 20 minutes.

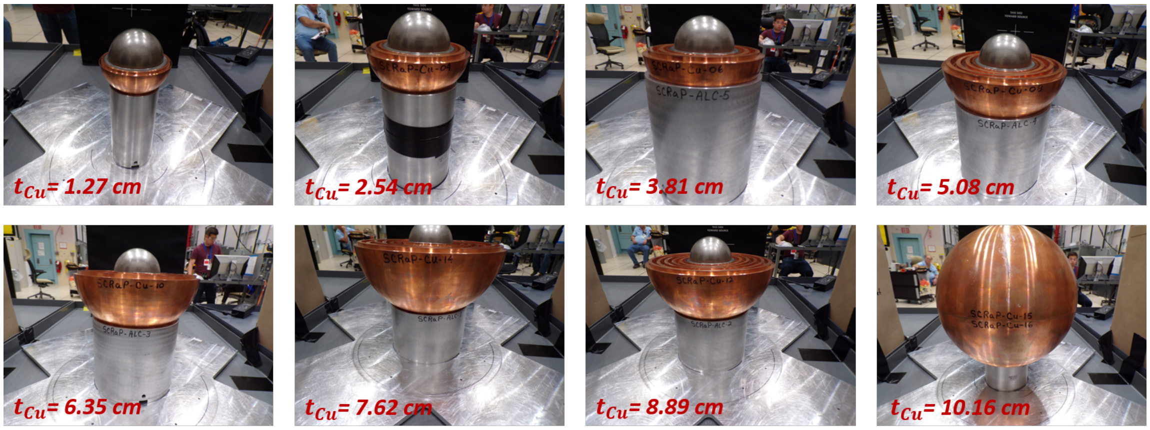

Figure 2: Photos of the BeRP Ball reflected by various copper thicknesses; the other half of the reflector shells are affixed during measurement.

The measured uranium radiation test object is made from shells of highly enriched uranium (HEU, 93.16% ^{235}U) known as the Rocky Flats shells [22, 23]. The composite shell is encased in aluminum for contamination control, made from Rocky Flats shells 3-30, has inner and outer HEU radii of 4.02 and 13.34 cm, and totals a mass of 21.6 kg. A rendering of the unencased shells that form the fissile core is shown in Fig. 3. A total of three configurations were measured: the core (shown in Fig 4), the core reflected by 3.81 cm of high-density polyethylene (HDPE), and the core reflected by 6.35 cm of HDPE. The assembly was driven by a ^{252}Cf source that was taped to the bottom of the assembly; the source-to-sample distance changes between configurations. Each configuration was measured for 30 minutes.

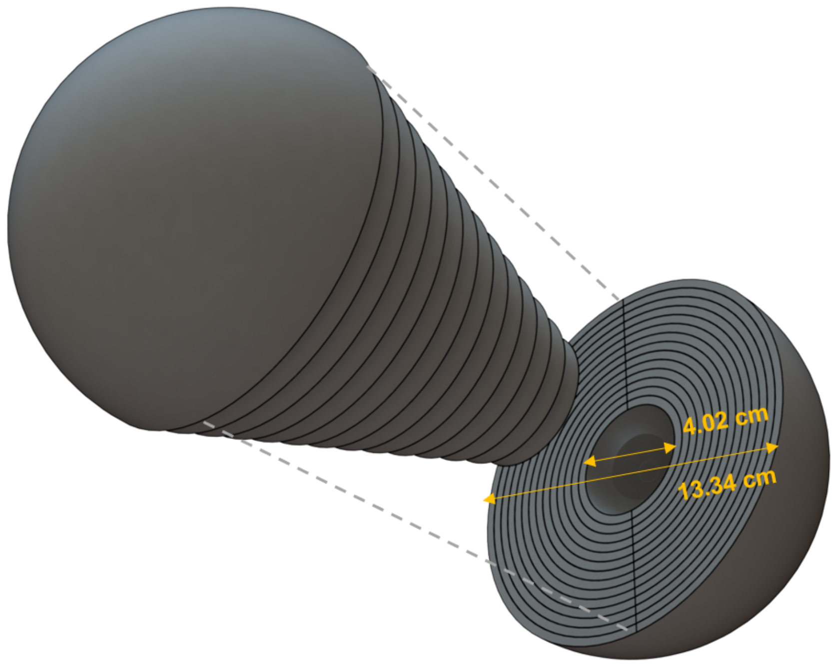

Figure 3: Three-dimensional rendering of Rocky Flats shells 3-30 with inner and outer radii of 4.02 and 13.34 cm.

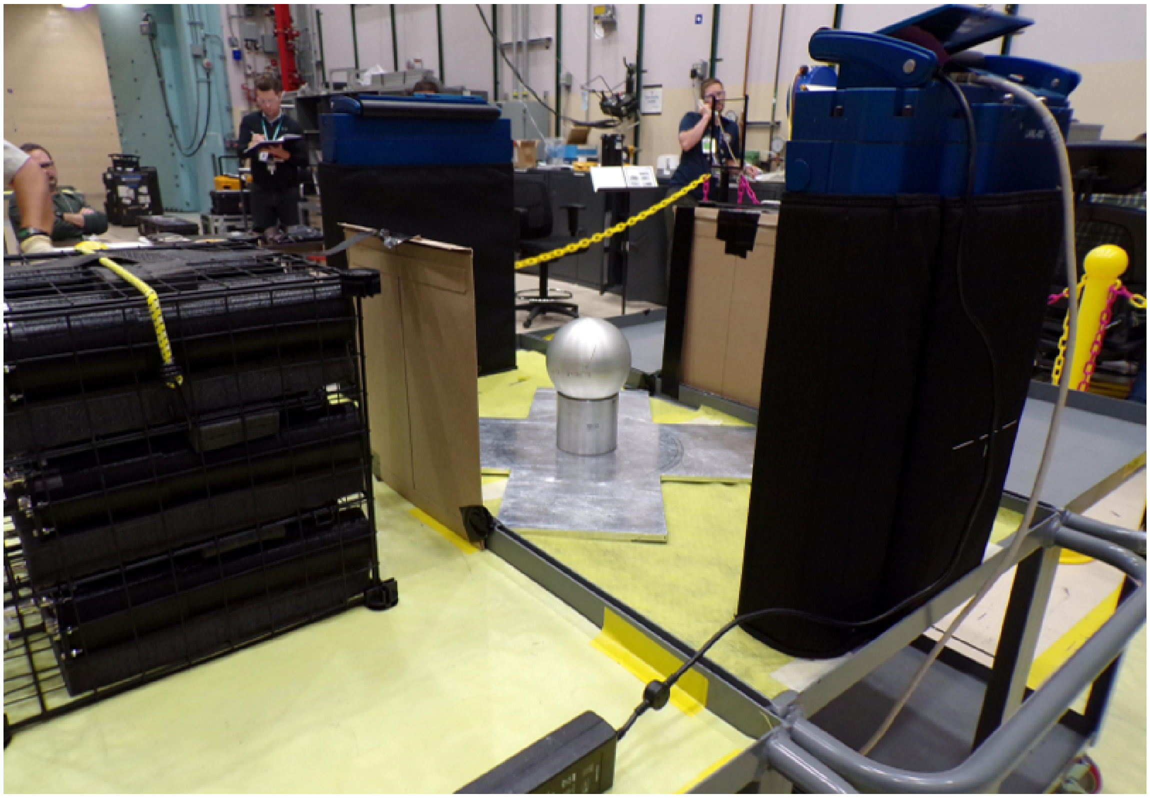

Figure 4: A photo of the measurement setup for the Rocky Flats experiment; in particular, the bare case is shown.

4. Data Analysis

Raw pulses from the detectors are preprocessed to eliminate clipped pulses (those resulting in more light output than allowed by the digitizer dynamic range based on calibration, or 2.39 MeVee in this work) and pulse pile-up (multiple pulses arriving in the same detector in the same 288 ns pulse window). Pulse shape discrimination (PSD) is used to distinguish neutron and photon pulses based on a charge integration technique for each detector, for each minute of measurement, and as a function of energy [24–26]. A sample PSD plot is shown in Fig. 5 for the measurement of the bare Rocky Flats assembly. The total integral range was the entire 288 ns pulse window, whereas the bounds for the tail integral started 24 ns after the pulse peak and extended to the end of the pulse.

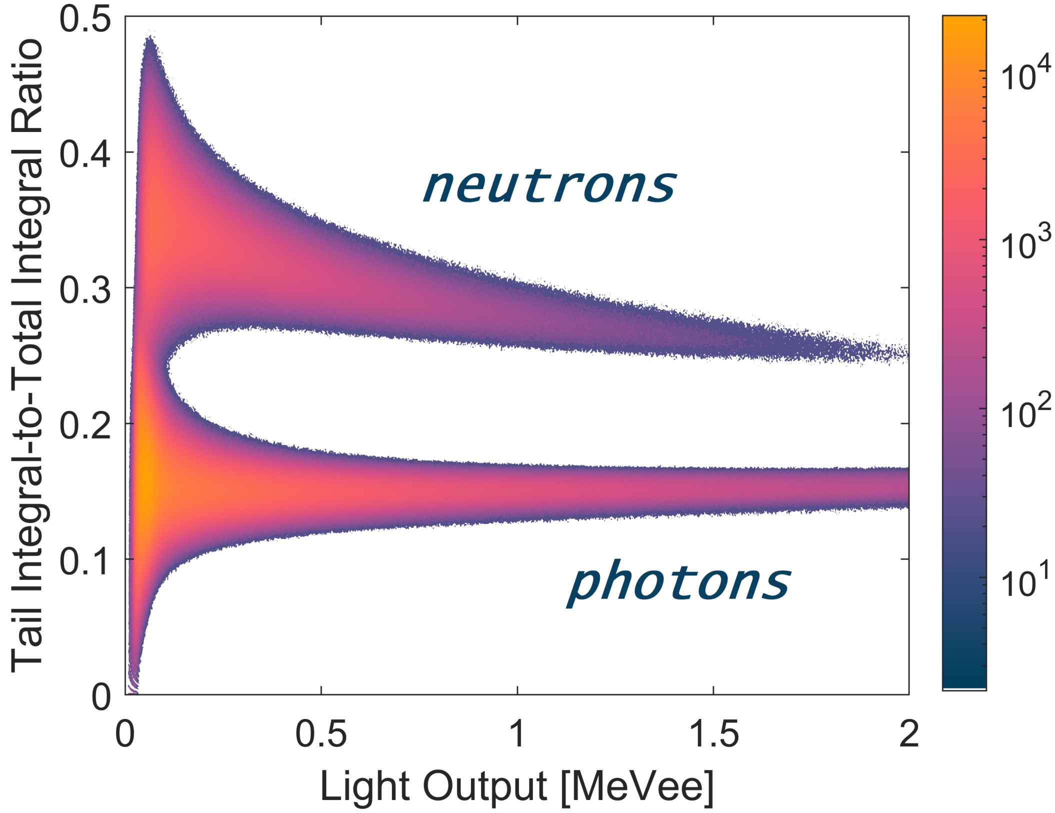

Figure 5: Sample pulse shape discrimination plot for the bare HEU assembly; the heat map has units of counts and illustrates relative intensity.

A list of neutron detection times and a list of photon detections times are obtained for each detector after the PSD algorithm finishes. Timing offsets due to electronics and differences in source-to-detector distance are corrected for by choosing a reference detector and calculating a photon time-difference distribution between the reference and any given detector. The list of times (for neutrons and for photons) in the given detector are translated by a constant such that the peak of the photon coincidence plot is centered about zero. The shift does not introduce significant bias in this work [14].

The Rossi-alpha distribution is constructed by creating a 1-ns bin-width histogram of any and all time differences between neutron detections in any detector, provided that the time differences are less than a 1000 ns reset time [6]. The constant representing uncorrelated counts, determined by taking the mean of the last 100 points in the distribution, is subtracted from the histogram. The first $2b+1$ points are omitted from the histogram to avoid effects such as dead time or neutron time-of-flight, where b is the index of the peak. The histogram is then fit with Eqn. (8) with the A term omitted (having already been determined and subtracted). The values of α and f' are calculated from Eqns. (9), (11), and (12).

The fit to the histogram is inverse-variance weighted. Ref. [27] presents formulations and validation for estimating bin-by-bin uncertainty for Rossi-alpha histograms, including sample and quasi-analytic methods. Ref. [28] also describes a bootstrapping method and demonstrates how to optimize histogram bin width and reset time for relative uncertainty and relative error. The sample method is used in this work. The nonlinear least squares, two-exponential fitting algorithm produces the Jacobian matrix in addition to the fit parameters. The Jacobian matrix is used to calculate the uncertainty in the fit parameters and propagate them to final estimates of α and f'. The entire process is derived and described in Ref. [27]. All error bars shown in this work are one standard deviation, σ.

There are three simulated parameters from the simulations of the experiments: k_{eff}, β_{eff}, and τ_c. The KCODE subroutine of MCNP6.2 is used to simulate the k_{eff} multiplication factors, which are used as reference values in this work. The KOPTS option was used to invoke calculation of β_{eff}. An F4 track-length tally for the plutonium and uranium cells weighted by inverse velocity and separately configured to calculate total progeny is used in a fixed-source calculation to estimate τ_c. A simulated value of α is calculated using the three simulated values, and a quasi-measured value of k_{eff} is calculated using the measured α and simulated β_{eff} and τ_c.

5. Experimental Validation Results and Discussion

The simulated reference values and measured values for the prompt neutron period for the copper-reflected plutonium assemblies are tabulated in Tab. 1. Table 1 also includes a column for the number of standard deviations for the means to overlap. The tabulated data are plotted in Fig. 6, and the table and figure are reproduced for k_{eff} instead of α in Tab. 2 and Fig. 7; however, the comparative column for k_{eff} shows relative error. The agreement between measurement and reference simulation improves as k_{eff} approaches unity; the trend is expected since the point kinetics models assume $k_{\text{eff}} \approx 1$. The measured and reference α values agree within one standard deviation for k_{eff} values above 0.9; similarly, the k_{eff} values agree in less than 5% error for k_{eff} values greater than 0.8831.

Table 1: Tabulated plutonium prompt neutron lifetime estimates $-\alpha^{-1}$ from measurement and reference values from simulation for validation.

Copper Thickness [cm]	Simulated [ns]		Measured [ns]		σ-Separation
	$-\alpha^{-1}$	$\sigma_{-\alpha^{-1}}$	$-\alpha^{-1}$	$\sigma_{-\alpha^{-1}}$	
1.27	7.6	0.2	13.4	1.0	4.91
2.54	12.5	0.4	19.5	1.0	4.97
3.81	17.9	0.9	27.6	4.0	1.99
5.08	25.0	2.3	32.1	4.9	1.00
6.35	33.7	3.5	40.8	7.4	0.65
7.62	40.5	6.2	43.6	5.1	0.28
8.89	60.7	4.8	68.8	3.6	0.96
10.16	73.4	8.6	75.6	4.5	0.17

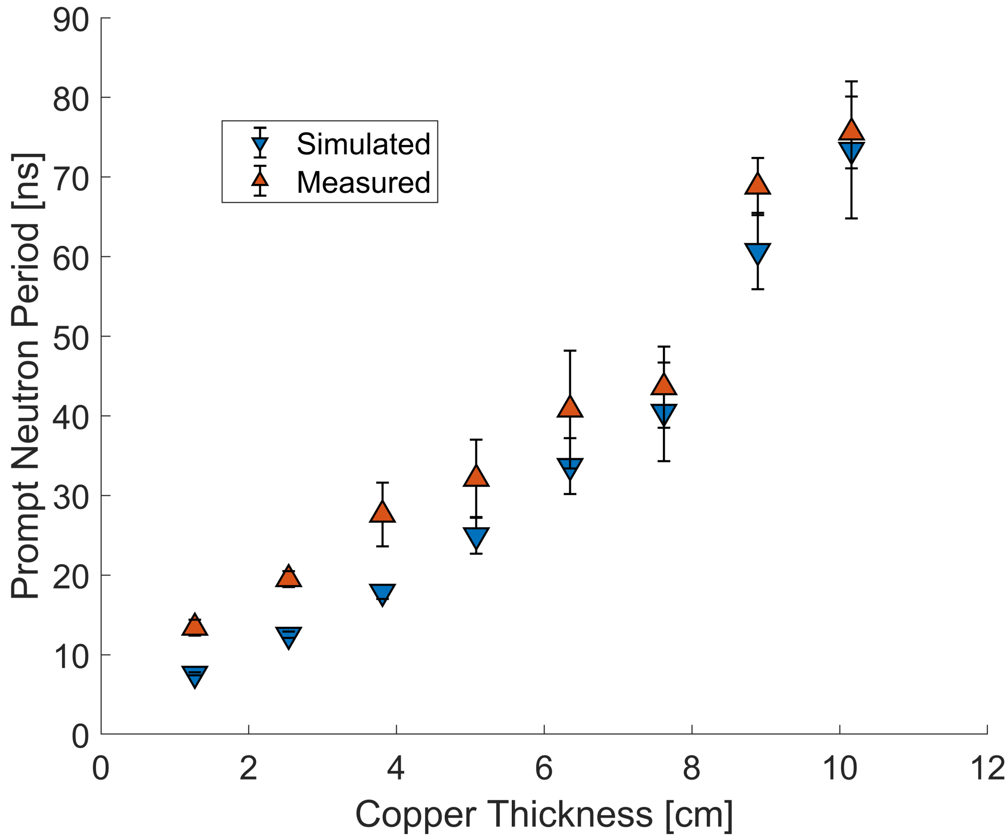

Figure 6: Simulated and measured prompt neutron periods for the BeRP Ball reflected by various amounts of copper.

Table 2: Tabulated plutonium k_{eff} estimates from measurement and reference values from simulation for validation.

Copper Thickness [cm]	Simulated		Measured		Error
	k_{eff}	$\sigma_{k_{\text{eff}}}$	k_{eff}	$\sigma_{k_{\text{eff}}}$	(M-S)/S
1.27	0.8278	0.0003	0.9045	0.0085	9.27%
2.54	0.8604	0.0003	0.9136	0.0071	6.18%
3.81	0.8831	0.0003	0.9271	0.0133	4.97%
5.08	0.9005	0.0003	0.9254	0.0168	2.77%
6.35	0.9137	0.0003	0.9309	0.0182	1.88%
7.62	0.9239	0.0003	0.9306	0.0176	0.73%
8.89	0.9322	0.0003	0.9411	0.0070	0.95%
10.16	0.9394	0.0003	0.9415	0.0093	0.22%

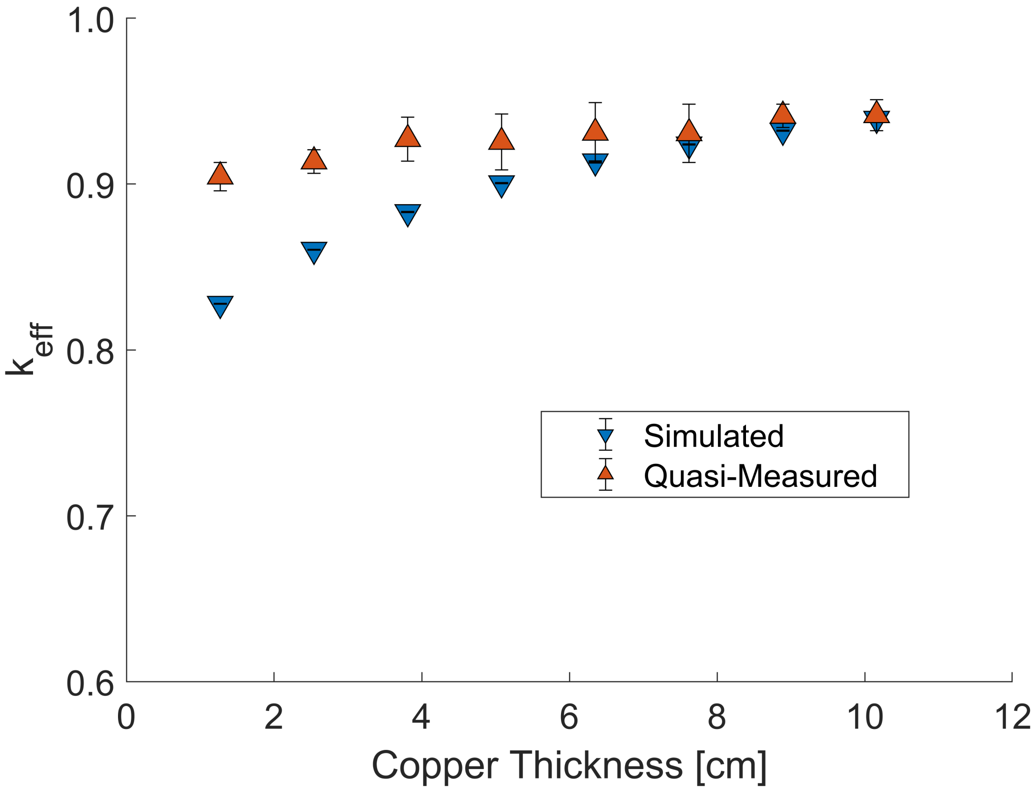

Figure 7: Comparison of quasi-measured k_{eff} to simulated reference values of k_{eff} for the copper-reflected plutonium measurements.

The prompt neutron period generally increases in a bare fissile core that increases k_{eff} by increasing in volume. A decreasing prompt neutron period (16.3, 13.3, 11.7 ns) as k_{eff} increased (0.7325, 0.9087, 0.9508) due to increased amounts of HDPE reflector (0.00, 3.81, 6.35 cm) was observed when analyzing the uranium data of this work. The trend was investigated by simulating the measured assemblies in MCNPX-PoliMi, observing the volumetric density of induced fission, and simulating track lengths/mean core lifetimes, which are summarized in Fig. 8. Photos of the assemblies are shown in Figs. 8a, 8b, and 8c; area-normalized heat maps of induced-fission density are shown in Figs. 8d, 8e, and 8f; and volume-normalized heat maps of induced-fission density are shown in Figs. 8g, 8h, and 8i. The area-normalized plots project the y-dimension data onto the x-z plane via summing, thus the void in the center of the assembly is visible. As the HDPE thickness and k_{eff} multiplication factor increase from Fig. 8d-8f, the bulk of induced fissions move from the center towards the cusp of the shell. The same transition is shown in the volume-normalized plots, which include annotations for τ_c and the mean track length in the core, λ_c, that decrease with increasing HDPE and k_{eff}. The trend is due to increased moderation of neutrons in the reflector (outside of the core) and, despite the neutrons being slower, ultimately shorter lifetimes in the core after reentry since the probability of induced fission significantly increases for moderated neutrons. The reducing prompt neutron period is therein verified. Furthermore, the reduction shows that increasingly thermal assemblies have faster core lifetimes and prompt neutron periods.

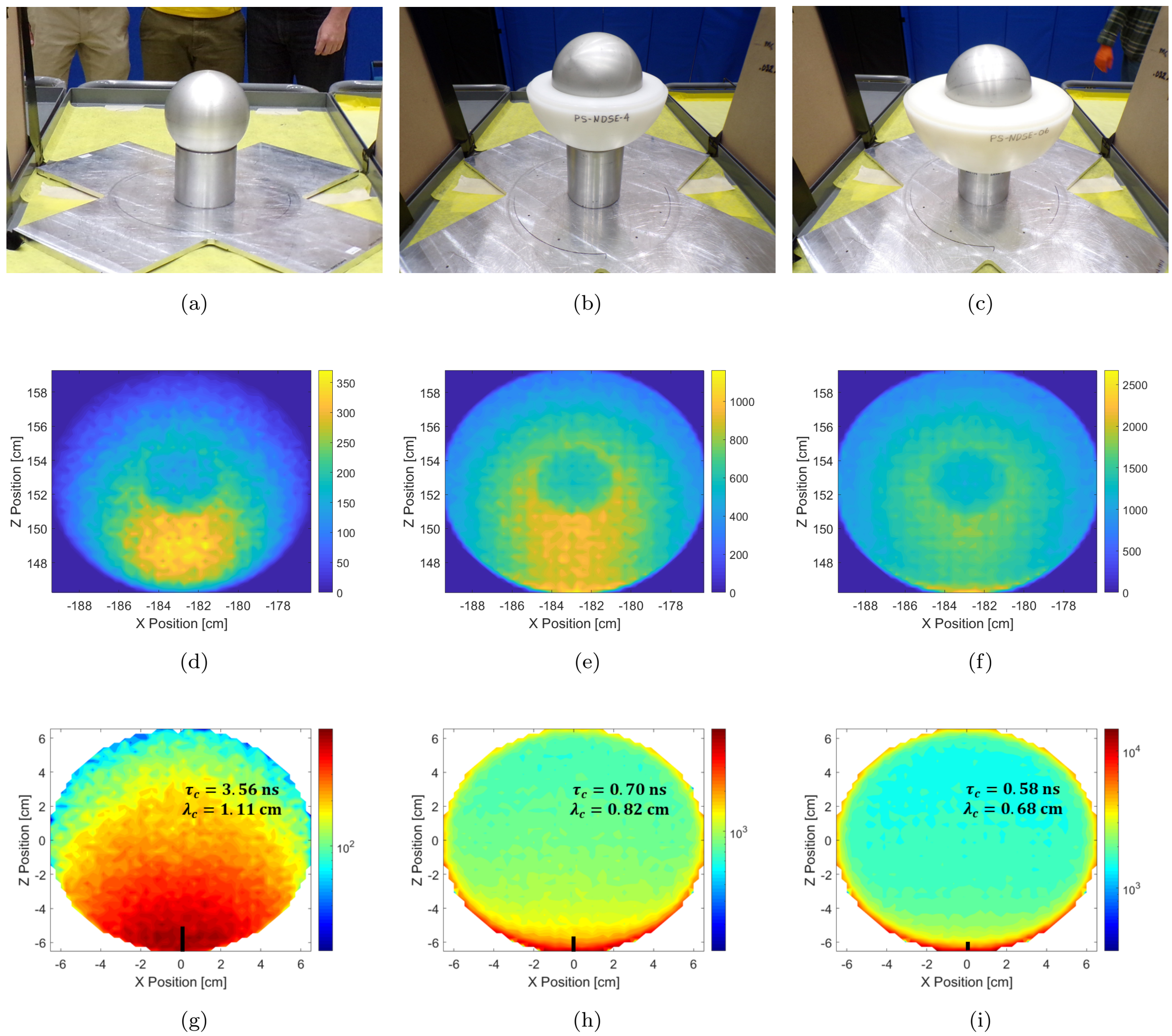

Figure 8: Photos of the aluminum-encased Rocky Flats shells (8a) bare, (8b) reflected by 3.81 cm of HDPE, and (8c) by 6.35 cm of HDPE; the other half of the reflector shells are affixed during measurement. The heat maps in the second and third row show the density of induced fission locations per area and per volume, respectively. Subfigs. (8d and 8g) correspond to the bare configuration, (8e and 8h) to the 3.81-cm-reflected configuration, and (8f and 8i) to the 6.35-cm-reflected configuration.

The verified prompt neutron periods, simulated effective delayed neutron fractions β_{eff}, and simulated prompt neutron lifetimes in the core τ_c were used to calculate quasi-measured k_{eff} values. The measured values of α were validated by comparing the quasi-measured k_{eff} to simulated reference values of k_{eff}, shown in Fig. 9 and tabulated in Tab. 3 with relative error. The relative error is again shown to decrease as k_{eff} tends to unity.

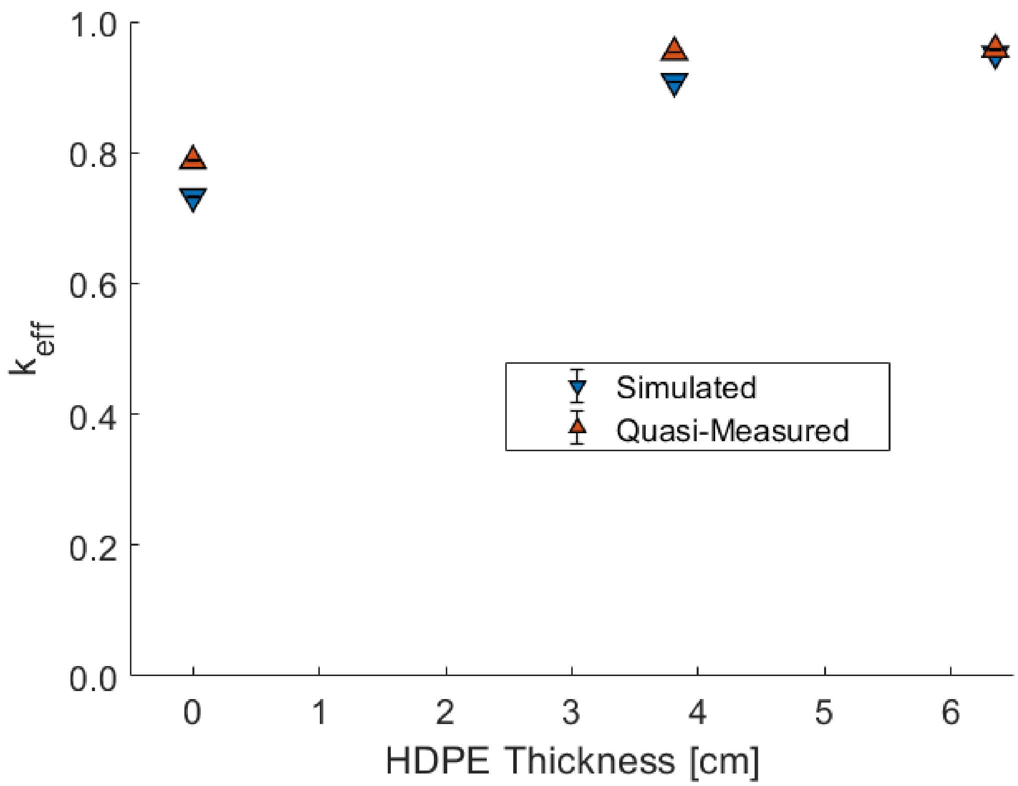

Figure 9: Comparison of quasi-measured k_{eff} to simulated reference values of k_{eff} for the HDPE-reflected HEU measurements.

Table 3: Tabulated uranium k_{eff} estimates from measurement and reference values from simulation for validation.

HDPE Thickness [cm]	Simulated		Measured		Error
	k_{eff}	$\sigma_{k_{\mathrm{eff}}}$	k_{eff}	$\sigma_{k_{\mathrm{eff}}}$	(M-S)/S
0.00	0.7325	0.0002	0.7947	0.0066	8.49%
3.81	0.9087	0.0004	0.9580	0.0018	5.43%
6.35	0.9508	0.0004	0.9603	0.0043	0.99%

6. Additional Signatures of Validated Two-Region Model

The two-region point kinetics model resulting in the two-exponential fits presents new measurable parameters, including the exponent-weighting parameter R. The purpose of this section is to study R with simulations of a moderated uranium assembly with MCNP6.2 [29] and MCNPX-PoliMi [30]. The simulated uranium assemblies are made from alternating spherical-shell layers of HEU (pure ^{235}U) and HDPE (0.97 g/cm^3) with an air-filled 2.25-cm sphere in the center. The total thicknesses of HEU and HDPE are 4.25 cm and 4.00 cm, respectively, and the HEU is always interior to the HDPE for a given layer. The configurations are designed to maintain a k_{eff} of 0.95 and vary the amount of reflection by increasing the number of alternating layers, N. The value of N is varied from 1 to 60 in addition to a homogeneous case ($N \to \infty$), and a constant k_{eff} is maintained by changing the HEU density (the HDPE density as well in the homogeneous case). Two-dimensional renderings of the simulation geometry for $N = 1, 2, \ldots, 5$ are shown in Fig. 10 and k_{eff} and density values are tabulated in Tab. 4. Fission chains were driven by an exterior, inward-facing, spherical-surface ^{252}Cf source.

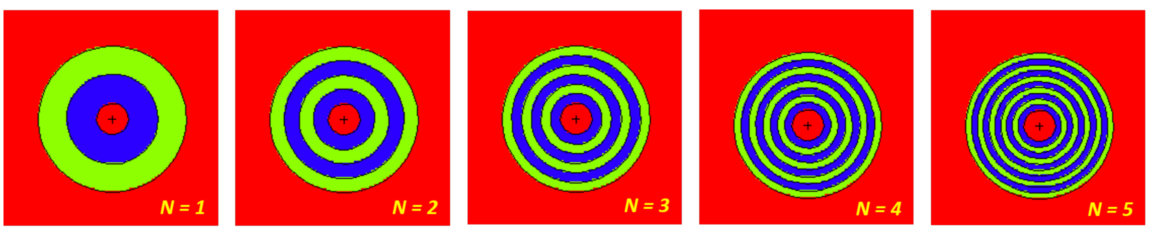

Figure 10: Two-dimensional rendering of sample geometries for the simulation study where N indicates the number of repeated HEU-HDPE layers. The blue layers are HEU and the green layers are HDPE.

Table 4: Approach-to-homogeneity simulation specifications and results. Densities are for the HEU regions only (HDPE density is fixed at 0.97 g/cm^3) except for the homogeneous case where there is one ^{235}U atom per CH_2. Values for $< E_n >$ are the mean neutron energy inducing fissions.

N	k_{eff}	$\sigma_{k_{\text{eff}}}$	HEU Density [g/cm^3]	R	$\langle E_n \rangle$ [MeV]
1	0.9496	0.0005	19.10	0.05	1.11
2	0.9497	0.0005	17.00	0.07	0.90
3	0.9499	0.0005	16.60	0.07	0.85
4	0.9499	0.0005	16.50	0.10	0.82
5	0.9489	0.0005	16.48	0.13	0.81
7	0.9497	0.0006	16.50	0.18	0.80
11	0.9501	0.0005	16.52	0.24	0.79
15	0.9500	0.0005	16.53	0.27	0.79
20	0.9496	0.0005	16.54	0.29	0.79
25	0.9497	0.0004	16.56	0.32	0.79
30	0.9495	0.0005	16.57	0.32	0.78
40	0.9494	0.0005	16.58	0.33	0.78
50	0.9502	0.0005	16.60	0.35	0.78
60	0.9501	0.0005	16.60	0.36	0.78
∞	0.9499	0.0006	8.75	0.39	0.75

In Eq. (11), R balances the two exponents of the fit to calculate α. As R approaches 0.5, the two-region model is more important; thus, between similar configurations, R could be an indicator of the type and amount of reflection for like assemblies. In the approach to homogeneity, the amount of reflection increases to maintain the same k_{eff}. A Rossi-alpha histogram was constructed for each N and treated with the two-exponential analysis to calculate R. The value of R as a function of the number of layers in the simulated assembly is shown in Fig. 11. Note that the order of the exponents can be switched such that R is always less than 0.5. The values of R asymptotically increase with the amount of reflection, approaching $R = 0.39$.

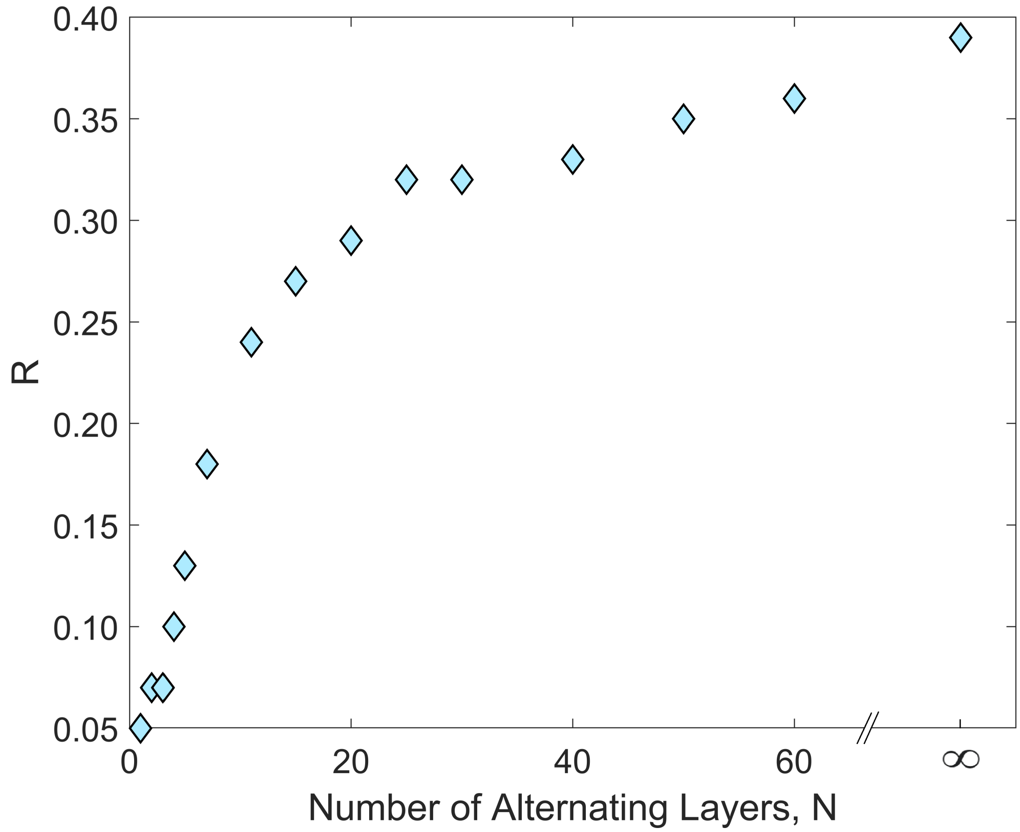

Figure 11: R parameter as a function of N, the number of alternating layers.

7. Summary, Conclusion, and Future Work

The two-exponential probability density function for Rossi-alpha experiments on reflected assemblies from two-region point kinetics is validated with organic scintillator measurements of copper-reflected plutonium and HDPE-reflected uranium. The agreement between measurement and simulation, which is used as the reference in this work, improves as k_{eff} approaches unity and is notably good above $k_{\text{eff}} = 0.9$. The trend in agreement for large k_{eff} is expected since point kinetics assumes $k_{\text{eff}} \approx 1$. The disagreement for small k_{eff} is also observed when directly comparing the prompt neutron periods, which is again expected. It is preferential to use the Rossi-alpha method when evaluating near- or delayed-critical assemblies and methods such as neutron multiplicity counting or the Feynman-Y method for deeply subcritical assemblies. The transition between methods is the subject of future work and the upcoming Measurement of Uranium Subcritical and Critical (MUSiC) benchmark [31, 32].

^{3}He detectors utilizing moderation cannot be used for two-region Rossi-alpha measurements unless the prompt neutron period of the core is larger than tens of microseconds and these large times cannot be achieved by making a system more thermal; the results show that increasingly thermal assemblies have shorter prompt neutron periods. Sufficiently large prompt neutron periods may occur for high k_{eff} multiplication factors; however, depending on the assembly, the associated large neutron fluxes may oversaturate and otherwise disqualify ^{3}He detectors. Future work will compare ^{3}He and organic scintillator systems for assemblies between delayed- and prompt-critical.

The mean neutron generation time Λ is traditionally used to infer k_{eff} in the one-region model. In the two-region model, either Λ of the core must be simulated (currently only Λ of the composite assembly is available in standard tools) to be paired with α of the core, α of the composite assembly must be measured (currently unavailable) to be used with the standard composite Λ, or the simulation of the mean neutron lifetime in the core τ_c approach of this work must be used. An experimentalist approach to measure a composite α may be to introduce a time constant (such as slowing down time) to the detection process (that does not affect the time correlations or behavior of the assembly) that is larger than both α and τ_r for detected neutrons. The data would then be treated with the two-exponential analysis and the smaller time constant that is calculated would correspond to the composite α. If assembly-decoupled moderator is added around the detectors for this approach, organic scintillators could not be used due to practical limits on detection threshold and the use of ^{3}He detectors may be preferential. This experimental approach is a hypothesis only and the subject of future feasibility tests.

Finally, a simulation study was performed to evaluate a newly available weighting parameter, R, that varies between zero and one. It was shown that R gets closer to 0.5 as reflection increases. The correlated behavior indicates that R could be used as a signature to infer reflector properties such as type and amount for similar assemblies. The value of R cannot necessarily be compared between substantially different assemblies since R is biased by the detected neutrons.

Acknowledgments

This work was partially supported by the National Science Foundation Graduate Research Fellowship under Grant No. DGE-1256260, the Consortium for Verification Technology under

Department of Energy National Nuclear Security Administration award number DE-NA0002534, the Consortium for Monitoring, Technology, and Verification under Department of Energy National Nuclear Security Administration award number DE-NA0003920, and the DOE Nuclear Criticality Safety Program, funded and managed by the National Nuclear Security Administration for the Department of Energy. Any opinion, findings, and conclusion or recommendations expressed in this material are those of the authors and do not necessarily reflect the views of any funding organization.

References

[1] R. Feynman, F. DeHoffmann, R. Serber, Statistical fluctuations in the water boiler and the dispersion of neutrons emitted per fission, LA-101, Los Alamos National Laboratory (1944).

[2] R. Feynman, F. DeHoffman, R. Serber, Intensity fluctuations of a neutron chain reactor, LADC-256, Los Alamos National Laboratory (1944).

[3] R. Feynman, F. D. Hoffmann, R. Serber, Dispersion of the neutron emission in U-235 fission, Journal of Nuclear Energy (1954) 3 (1) (1956) 64 – IN10. doi:https://doi.org/10.1016/0891-3919(56)90042-0.

[4] R. Uhrig, U. A. E. Commission, Random noise techniques in nuclear reactor systems, Ronald Press, 1970.

[5] J. Orndoff, Prompt neutron periods of metal critical assemblies, Nuclear Science and Engineering 2 (4) (1957) 450–460.

[6] G. E. Hansen, The rossi alpha method, Los Alamos National Laboratory, Technical Report (LA-UR-85-4176) (8 1985).

[7] J. T. Mihalczo, Prompt neutron decay and reactivity measurements in subcritical uranium metal cylinders, Nuclear Science and Engineering 32 (3) (1968) 292–301. doi:10.13182/NSE68-A20211.

[8] J. Hutchinson, G. McKenzie, J. Arthur, M. Nelson, W. Monage, Prompt neutron decay constant fitting using the rossi-alpha and feynman variance-to-mean methods, Transactions of the American Nuclear Society 117 (2017) 986–989.

[9] R. Kuramoto, A. dos Santos, R. Jerez, R. Diniz, U. Bitelli, T. Madi Filho, C. Luis Veneziani, Rossi-α experiment in the IPEN/MB-01 research reactor: Validation of two-region model and absolute measurement of β_{eff} and Λ 2006 (01 2006).

[10] R. Avery, Coupled fast-thermal power breeder, Nuclear Science and Engineering 3 (2) (1958) 129–144. doi:10.13182/NSE58-A25455.

[11] C. E. Cohn, Reflected-Reactor Kinetics, Nuclear Science and Engineering 13 (1) (1962) 12–17. doi:10.13182/NSE62-A26122.

[12] M. Y. Hua, J. D. Hutchinson, G. E. McKenzie, T. H. Shin, S. D. Clarke, S. A. Pozzi, Derivation of the two-exponential probability density function for rossi-alpha measurements of reflected assemblies and validation for the special case of shielded measurements, Nuclear Science and Engineering 194 (1) (2020) 56–68. doi:10.1080/00295639.2019.1654327.

[13] K. Ott, R. Neuhold, Introductory nuclear reactor dynamics, American Nuclear Society, 1985.

[14] M. Y. Hua, C. A. Bravo, A. T. MacDonald, J. D. Hutchinson, G. E. McKenzie, B. C. Kiedrowski, S. D. Clarke, S. A. Pozzi, Rossi-alpha measurements of fast plutonium metal assemblies using organic scintillators, Nuclear Instruments and Methods in Physics Research Section A: Accelerators, Spectrometers, Detectors and Associated Equipment 959 (2020) 163507. doi:https://doi.org/10.1016/j.nima.2020.163507.

[15] J. Hutchinson, R. Bahran, T. Cutler, J. Arthur, M. Nelson, Subcritical copper-reflected alpha-phase plutonium (SCRaP) measurements and simulations, M&C 2017 - International Conference on Mathematics & Computational Methods Applied to Nuclear Science & Engineering (2017).

[16] N. Zaitseva, A. Glenn, L. Carman, H. P. Martinez, R. Hatarik, H. Klapper, S. Payne, Scintillation properties of solution-grown trans-stilbene single crystals, Nuclear Instruments and Methods in Physics Research Section A: Accelerators, Spectrometers, Detectors and Associated Equipment 789 (2015) 8 – 15. doi:https://doi.org/10.1016/j.nima.2015.03.090.

[17] M. Bourne, S. Clarke, N. Adamowicz, S. Pozzi, N. Zaitseva, L. Carman, Neutron detection in a high-gamma field using solution-grown stilbene, Nuclear Instruments and Methods in Physics

Research Section A: Accelerators, Spectrometers, Detectors and Associated Equipment 806 (2016) 348 – 355. doi:https://doi.org/10.1016/j.nima.2015.10.025.

[18] J. Mattingly, Polyethylene-reflected plutonium metal sphere: subcritical neutron and gamma measurements. (11 2009). doi:10.2172/974870.

[19] E. Miller, B. Dennis, S. Clarke, S. Pozzi, J. Mattingly, Simulation of polyethylene-moderated plutonium neutron multiplicity measurements, Nuclear Instruments and Methods in Physics Research Section A: Accelerators, Spectrometers, Detectors and Associated Equipment 652 (1) (2011) 540 – 543, symposium on Radiation Measurements and Applications (SORMA) XII 2010. doi:https://doi.org/10.1016/j.nima.2011.01.042.

[20] B. Richard, J. Hutchinson, Nickel reflected plutonium metal sphere subcritical measurements, In: International Handbook of Evaluated Criticality Safety Benchmark Experiments [DVD]/Nuclear Energy Agency. - Paris : OECD Nuclear Energy Agency, (NEA;7328) (2016).

[21] B. Richard, J. Hutchinson, Tungsten-reflected plutonium-metal-sphere subcritical measurements, In: International Handbook of Evaluated Criticality Safety Benchmark Experiments [DVD]/Nuclear Energy Agency. - Paris : OECD Nuclear Energy Agency, (NEA;7328) (2016).

[22] R. Rothe, Extrapolated experimental critical parameters of unreflected and steel-reflected massive enriched uranium metal spherical and hemispherical assemblies (INEEL/EXT–97-01401). doi:10.2172/658339.

[23] J. A. Gomez, P. E. Koehler, T. E. Cutler, A. DeYoung, J. T. Goorley, J. D. Hutchinson, G. McKenzie, G. L. Morgan, S. M. Mosby, W. L. Myers, R. S. Rundberg, V. W. Yuan, Results of three neutron diagnosed subcritical experiments, Nuclear Science and Engineering 193 (5) (2019) 537–548. doi:10.1080/00295639.2018.1545956.

[24] F. Brooks, A scintillation counter with neutron and gamma-ray discriminators, Nuclear Instruments and Methods 4 (3) (1959) 151 – 163. doi:10.1016/0029-554X(59)90067-9.

[25] L. F. Miller, J. Preston, S. Pozzi, M. Flaska, J. Neal, Digital pulse shape discrimination, Radiation Protection Dosimetry 126 (1-4) (2007) 253–255. doi:10.1093/rpd/ncm052.

[26] J. Polack, M. Flaska, A. Enqvist, C. Sosa, C. Lawrence, S. Pozzi, An algorithm for charge-integration, pulse-shape discrimination and estimation of neutron/photon misclassification

in organic scintillators, Nuclear Instruments and Methods in Physics Research Section A: Accelerators, Spectrometers, Detectors and Associated Equipment 795 (2015) 253 – 267. doi:https://doi.org/10.1016/j.nima.2015.05.048.

[27] M. Y. Hua, J. D. Hutchinson, G. E. McKenzie, B. C. Kiedrowski, M. W. Liemohn, S. D. Clarke, S. A. Pozzi, Measurement uncertainty of rossi-alpha neutron experiments, Annals of Nuclear Energy 147 (2020) 107672. doi:https://doi.org/10.1016/j.anucene.2020.107672.

[28] M. Y. Hua, J. D. Hutchinson, G. E. McKenzie, M. A. Nelson, Rossi-alpha uncertainty quantification by analytic, bootstrap, and sample methods to inform fitting best practices, Transactions of the American Nuclear Society (11 2020).

[29] C. J. Werner, J. S. Bull, C. J. Solomon, F. B. Brown, G. W. McKinney, M. E. Rising, D. A. Dixon, R. L. Martz, H. G. Hughes, L. J. Cox, A. J. Zukaitis, J. C. Armstrong, R. A. Forster, L. Casswell, MCNP version 6.2 release notesdoi:10.2172/1419730.

[30] S. A. Pozzi, E. Padovani, M. Marseguerra, Mcnp-polimi: a monte-carlo code for correlation measurements, Nuclear Instruments and Methods in Physics Research Section A: Accelerators, Spectrometers, Detectors and Associated Equipment 513 (3) (2003) 550 – 558. doi:https://doi.org/10.1016/j.nima.2003.06.012.

[31] A. T. McSpaden, T. E. Cutler, J. D. Hutchinson, G. E. McKenzie, Finalization of the IER 488 (MUSiC) experiment design, Nuclear Criticality Safety Program (NCSP) Technical Program Review (3 2019).

[32] R. A. Weldon, T. E. Cutler, J. D. Hutchinson, W. L. Myers, G. E. McKenzie, A. T. McSpaden, R. G. Sanchez, Application of the rossi-alpha method to simulations of HEU and organic scintillators, Transactions of the American Nuclear Society (11 2020).